Acta Oceanol. Sin., 2015, Vol. 34, No. 9, P. 58–64
DOI: 10.1007/s13131-015-0738-0
http://www.hyxb.org.cn
E-mail: hyxbe@263.net

The seasonal variations in the significant wave height and sea surface wind speed of the China's seas

ZHENG Chongwei[1, 2, 3]*, PAN Jing[2], TAN Yanke[1], GAO Zhansheng[3], RUI Zhenfeng[3], CHEN Chaohui[1]

[1] College of Meteorology and Oceanography, People's Liberation Army University of Science and Technology, Nanjing 211101, China

[2] National Key Laboratory of Numerical Modeling for Atmospheric Sciences and Geophysical Fluid Dynamics (LASG), Institute of Atmospheric Physics, Chinese Academy of Sciences, Beijing 100029, China

[3] Dalian Naval Academy, Dalian 116018, China

Received 1 October 2014; accepted 4 March 2015

Abstract

Long-term variations in a sea surface wind speed (WS) and a significant wave height (SWH) are associated with the global climate change, the prevention and mitigation of natural disasters, and an ocean resource exploitation, and other activities. The seasonal characteristics of the long-term trends in China's seas WS and SWH are determined based on 24 a (1988–2011) cross-calibrated, multi-platform (CCMP) wind data and 24 a hindcast wave data obtained with the WAVEWATCH-III (WW3) wave model forced by CCMP wind data. The results show the following. (1) For the past 24 a, the China's WS and SWH exhibit a significant increasing trend as a whole, of 3.38 cm/(s·a) in the WS, 1.3 cm/a in the SWH. (2) As a whole, the increasing trend of the China's seas WS and SWH is strongest in March-April-May (MAM) and December-January-February (DJF), followed by June-July-August (JJA), and smallest in September-October-November (SON). (3) The areal extent of significant increases in the WS was largest in MAM, while the area decreased in JJA and DJF; the smallest area was apparent in SON. In contrast to the WS, almost all of China's seas exhibited a significant increase in SWH in MAM and DJF; the range was slightly smaller in JJA and SON. The WS and SWH in the Bohai Sea, the Yellow Sea, East China Sea, the Tsushima Strait, the Taiwan Strait, the northern South China Sea, the Beibu Gulf, and the Gulf of Thailand exhibited a significant increase in all seasons. (4) The variations in China's seas SWH and WS depended on the season. The areas with a strong increase usually appeared in DJF.

Key words: sea surface wind speed, significant wave height, long-term variation, seasonal difference

Citation: Zheng Chongwei, Pan Jing, Tan Yanke, Gao Zhansheng, Rui Zhenfeng, Chen Chaohui. 2015. The seasonal variations in the significant wave height and sea surface wind speed of the China's seas. Acta Oceanologica Sinica, 34(9): 58–64, doi: 10.1007/s13131-015-0738-0

1 Introduction

The long-term variation in the ocean environment is associated with the global climate change, the prevention and mitigation of natural disasters, and the ocean resource exploitation, among other activities (Huang et al., 2011). The climate changes in the WS and the SWH greatly affect coastal populations (Soomere and Raamet, 2011; Suarez et al., 2013; Zheng, Shao et al., 2014; Zheng, Pan et al., 2014; Han et al., 2014; Zheng, Jiang et al., 2014; Ren et al., 2015); thus, it is necessary to evaluate the long-term trends in these features.

Many excellent studies on the variation in the WS and SWH have been presented by previous researchers. Gower (2002) stated that both the Northeast Pacific WS and SWH exhibit a significant increase of approximately 1–5 cm/(s·a) and 1–4 cm/a, respectively, according to the buoy data. Gulev and Grigorieva (2006) found that the winter SWH in the north Pacific and North Atlantic midlatitudes exhibited a significant increase of 10–40 cm/decade over the past 45 a using International Comprehensive Ocean-Atmosphere Data Set (ICOADS) data. Young et al. (2011) found a global increase in the WS and SWH over the past 23 a based on a database of calibrated and validated satellite altimeter measurements. Guillaume et al. (2010) found that SWH linearly increased (approximately 2 cm/a) in the Northeast Atlantic during 1953–2009 using a third-generation wave model. Utilizing 45 a of the European Centre for Medium-Range Weather Forecasts (ECMWF) reanalysis (ERA-40) wave data, Zheng, Zhou et al. (2013) discovered that a majority of the global ocean swell wave heights exhibit a significant linear increase (0.2–0.8 cm/a). There is good agreement between the long-term trend in the SWH and the trend in the swell wave height.

However, there are few studies on the overall climatic trends of the China's seas WS and SWH and on the seasonal characteristics of the climatic trends. In the process of ocean engineering or the development of an ocean energy, we usually focus on the seasonal characteristics of the long-term trends in the WS and SWH, which are related to planning in different seasons. In this study, we present the seasonal characteristics of the long-term trends in the China's seas WS and SWH based on 24 a (1988–2011) cross-calibrated, multi-platform (CCMP) wind data and the 24 a hindcast wave data obtained with the WAVE-

Foundation item: The National Basic Research Program of China under contract Nos 2015CB453200, 2013CB956200, 2012CB957803 and 2010CB950400; the National Natural Science Foundation of China under contract Nos 41275086 and 41475070.
*Corresponding author, E-mail: chinaoceanzcw@sina.cn

WATCH-III (WW3) wave model forced by the CCMP wind data. The objective is to provide a reference for wave energy resources development, the marine engineering, and the disaster prevention and mitigation.

2 Method and data

2.1 *Method*

In this study, a 24 a CCMP wind data set and a 24 a hindcast wave data set were used to analyze the long-term trends in the China's seas (including the Bohai Sea, the Yellow Sea, the East China Sea and the South China Sea, topography is shown in Fig. 1) WS and SWH. The overall variations in the SWH and the WS are presented. We first calculated the seasonal variations.

2.2 *Wind data*

The CCMP ocean surface wind product is hosted by the Physical Oceanography Distributed Active Archive Center (PO.DAAC), and it has been evaluated and utilized extensively by the science community (Atlas et al., 2011). The data are derived through cross-calibration and assimilation of the ocean surface wind data from SSM/I, TMI, AMSR-E, SeaWinds on QuikSCAT, and SeaWinds on ADEOS-II. The temporal resolution of the CCMP wind data is 6 h (July 1987 to July 2011), and the spatial resolution is 0.25°×0.25° (78.375°S–78.375°N, 0.125°–359.875°E). The CCMP ocean surface wind product is widely used (Zheng and Pan, 2014).

Available at http://rda.ucar.edu/datasets/ds744.9/.

2.3 *Wave data*

The WW3 wave model was used to simulate the China's seas wave field forced by the CCMP wind data. To eliminate the boundary effect and improve the precision of the simulated wave data, we set the simulation area as 3.875°S–41.125°N, 97.125°–135.125°E and then extracted 0°–40°N, 100°–130°E, which contains the main part of the China's seas and surrounding waters. The spatial resolution is 0.25°×0.25°, and the time step is 900 s (output every 3 h). The model time is 00:00 January 1, 1988, to 18:00 December 31, 2011.

Contrasting these data with buoy data from the Japan SATA Cape, Fukue Island and Korea Cheju Island, we found consistency between the simulated wave data and the observed data (Zheng, Pan et al., 2013). Past studies also show that the WW3 has the ability to simulate wave fields in the China's seas (Chu et al., 2004; Mirzaei et al., 2013). In conclusion, the simulated wave data in this study are reliable.

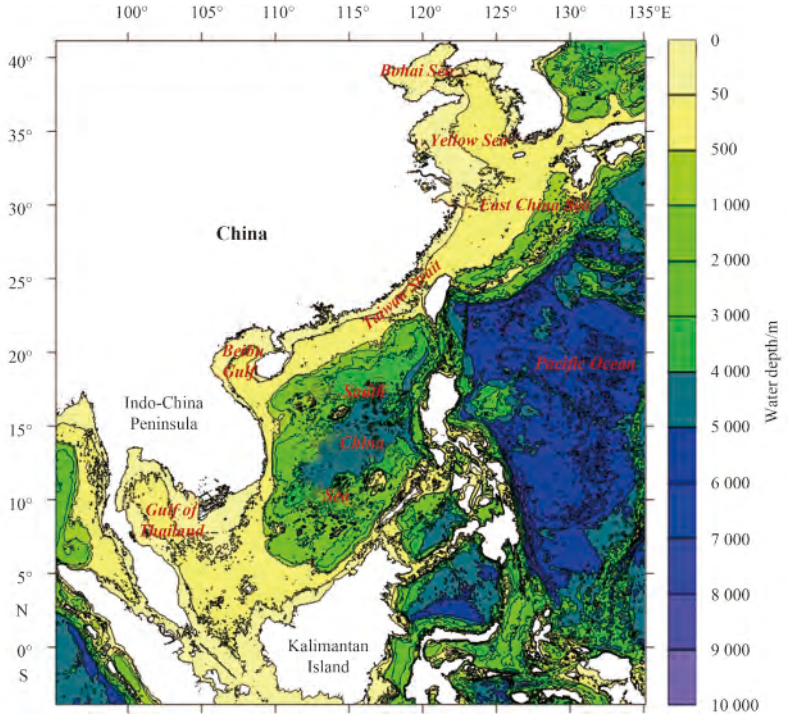

Fig. 1. Topography of the China's seas and surrounding waters.

3 Long-term trends in SWH and WS

3.1 *Overall trends in the annual average SWH and WS*

By calculating the regional average WS from 00:00 UTC on January 1, 1988, to 18:00 UTC on December 31, 1988, a yearly average WS was obtained. Using the same method, we obtained 24 regional and yearly average values of the China's seas WS to analyze the overall long-term trend for 1988–2011, as shown in Fig. 2a. Using the same method, the overall variation in the China's seas SWH was also analyzed, as shown in Fig. 2b.

From Fig. 2, we found a similar curve between the China's seas WS and SWH for the past 24 a because the China's seas are located along the edge of the northwest Pacific. The swell index near the shore was much smaller than that offshore; therefore, the sea was directly affected by the wind field and was dominated by mixed waves (Zheng, Zhou et al., 2013).

As shown in Fig. 2a, the correlation coefficient (denoted by r) of the WS is 0.82, which is significant at the 99% level. The regression coefficient is 0.033 8. Specifically, the China's seas WS exhibited a significant increase of 3.38 cm/(s·a) over 1988–2011. Similarly, the China's seas SWH (Fig. 2b) exhibited a significant increase of 1.3 cm/a over the past 24 years.

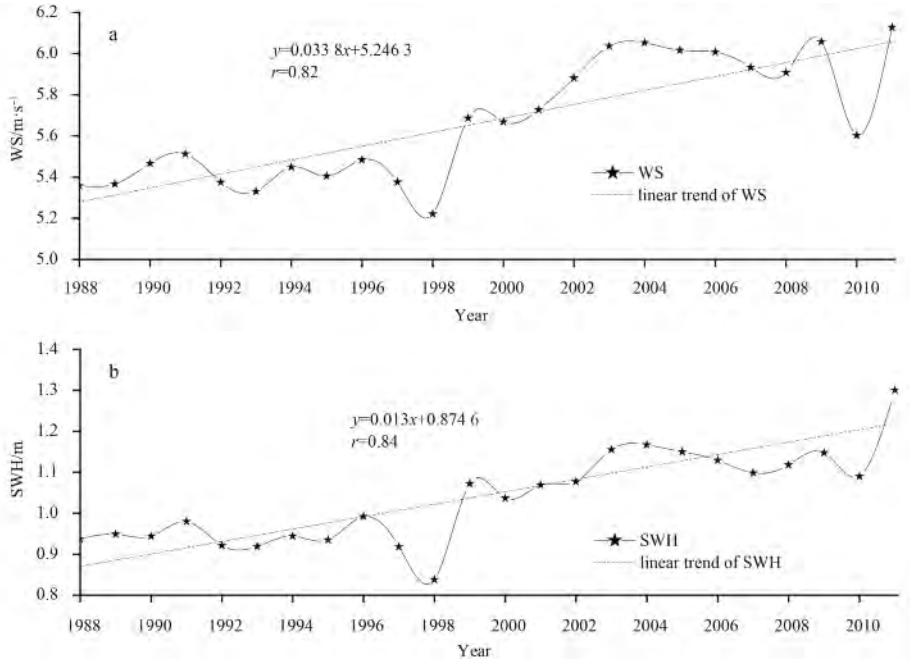

Fig. 2. Annual long-term trends in the China's seas surface WS (a) and SWH (b).

During 1988–1996, the annual average WS of 5.35 m/s changed gradually. After 1996, the WS decreased rapidly and then dropped to a minimum of 5.20 m/s in 1998. From 1998 to 2003, the China's seas WS increased rapidly. Over 2004–2011, the variation was relatively stable. The year of 2010 was unusual due to its low winds. Likewise, Earl et al. (2013) noted that 2010 was an anomalously low wind year. The curves for the China's seas SWH and WS were very consistent each year except in 2010.

3.2 *Overall trend in different seasons*

By calculating the regional average WS from 00:00 UTC on March 1, 1988, to 18:00 UTC on May 31, 1988, a seasonal average WS in MAM of 1998 was obtained. Using the same method, we obtained 24 values for the China's seas WS each MAM over 1988–2011. Then, the variation in the China's seas WS in MAM was analyzed, as shown in Fig. 3a. Using the same method, the overall trends in the China's seas WS in JJA, SON and DJF are also presented, as shown in Fig. 3. Similarly, the overall trends in the China's seas SWH in MAM, JJA, SON and DJF are also presented, as shown in Fig. 4.

From Fig. 3a, the correlation coefficient is 0.88, which is significant at the 99% level. The regression coefficient was 0.041 9. Specifically, the China's seas WS exhibited a significant increase of 4.19 cm/(s·a) in MAM over 1988–2011. Similarly, the China's seas WS exhibited a significant increase of 3.21 cm/(s·a) in JJA, 2.42 cm/(s·a) in SON, and 3.82 cm/(s·a) in DJF. We also found that the increase in the China's seas WS was strongest in MAM, followed by DJF, JJA, and SON.

From Fig. 4, clearly, the China's seas SWH exhibited a significant increase of 1.71 cm/a in MAM, 1.25 cm/a in JJA, 1.20 cm/a in SON, and 1.82 cm/a in DJF. The increase in the China's seas SWH was strongest in DJF, followed by MAM, JJA, and SON.

3.3 *Seasonal differences in the long-term trends in different water bodies*

To present the seasonal differences in different water bodies, this study calculated the long-term trends in China's seas SWH and WS for every 0.25°×0.25° grid point in MAM, JJA, SON and DJF, as shown in Fig. 5.

3.3.1 *Long-term trends in the WS in MAM, JJA, SON and DJF*

As shown in Figs 5a–d, the long-term trend in the WS in the China's seas showed great seasonal differences. The areal extent of the significant speed increase was largest in MAM; the area decreased in JJA and DJF, with the smallest area in SON. The WS in the Bohai Sea, the Yellow Sea, the East China Sea, the Tsushima Strait, the Taiwan Strait, the northern South China Sea, the Beibu Gulf, and the Gulf of Thailand exhibited a significant increase in all seasons, while only a few sporadic water bodies showed a significant decreasing trend.

In MAM, most China's seas showed a significant increase above 3 cm/(s·a). Areas with a relatively strong increase were located in the Tsushima Strait (15–18 cm/(s·a)), around Taiwan (9–18 cm/(s·a)), around the Ryukyu Islands (6 cm/(s·a)) and the northern South China Sea (above 6 cm/(s·a)).

In JJA, areas with a significant increase were mainly distributed in large water bodies to the north of 15° N, the Gulf of Thailand and around Kalimantan. The peak-value areas were located in the Tsushima Strait (6–12 cm/(s·a)), around Taiwan (3–12 cm/(s·a)), the Beibu Gulf (above 6 cm/(s·a)) and the Gulf of Thailand (above 9 cm/(s·a)).

In SON, there were a few small regions with a significant increase in the WS. These areas were mainly distributed in the Bohai Sea, the Yellow Sea, areas to the north of 25°N in the East China Sea, the northern South China Sea and the Gulf of Thailand.

The variation in the WS in DJF was similar to that in SON to a certain extent, while the area with a significant increase was greater than that in SON.

3.3.2 *Long-term trends in SWH in MAM, JJA, SON and DJF*

As shown in Figs 5e–h, the long-term trend in the China's seas SWH also showed noticeable seasonal differences. In contrast to the WS, almost all China's seas SWH values exhibited sig-

nificant increases in MAM and DJF, and the range was slightly smaller in JJA and SON. The SWH in the Bohai Sea, the Yellow Sea, the East China Sea, the Tsushima Strait, the Taiwan Strait, the northern South China Sea, the Beibu Gulf, and the Gulf of Thailand exhibited a significant increase in all seasons, while only a few sporadic water bodies showed a significant decrease.

In MAM, almost the entire China's seas exhibited a significant increase greater than 0.5 cm/a. The areas with a strong increase were located in the Tsushima Strait (approximately 2.5 cm/a), the Ryukyu Islands waters (approximately 2.0 cm/a) and most of the South China Sea (above 1.5 cm/a), particularly in the waters of the Dongsha Islands, where the long-term trend increased to 3.0 cm/a.

In JJA, the SWH had a significant increase in most waters to

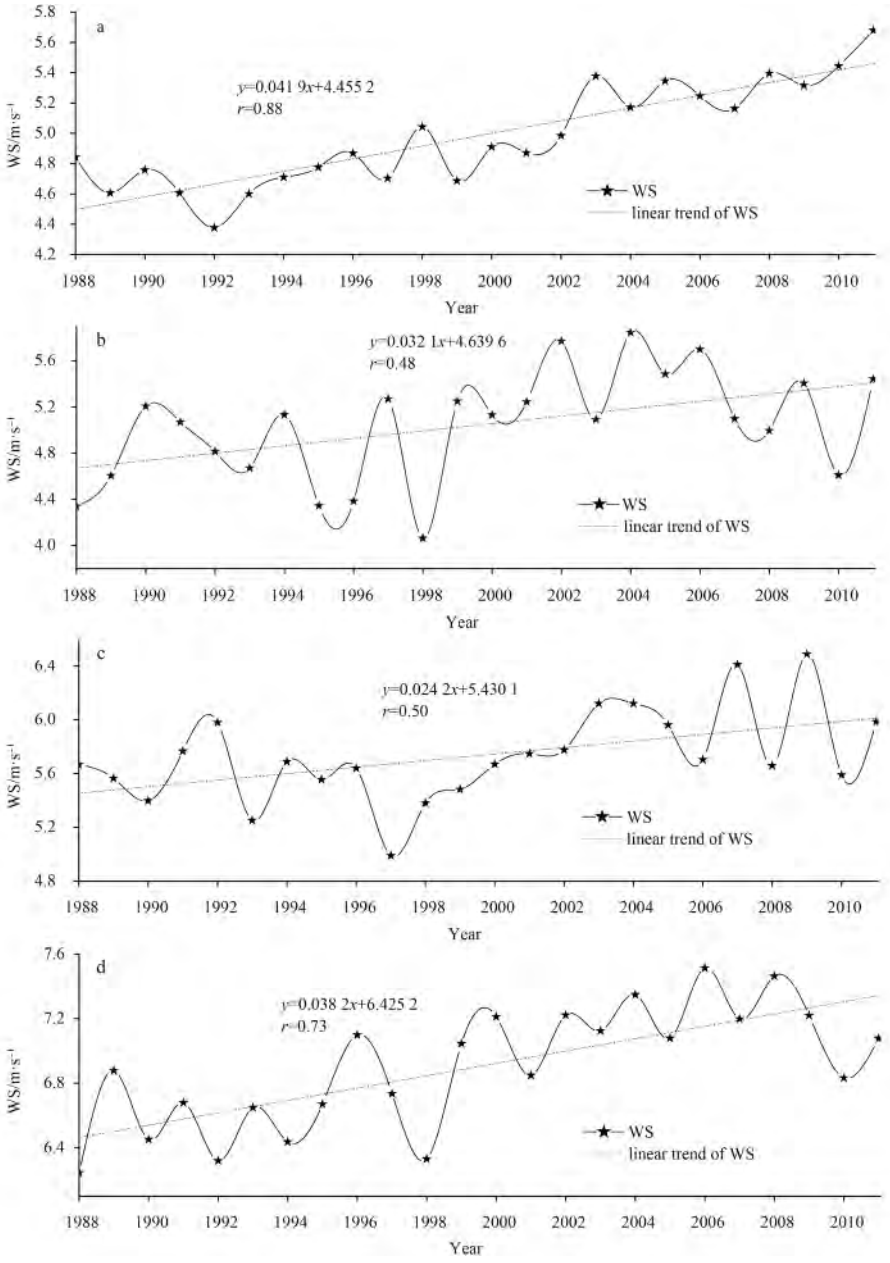

Fig. 3. Long-term trends in the China's seas surface WS in MAM (a), JJA (b), SON (c) and DJF (d).

the north of 15°N, the Gulf of Thailand and the waters surrounding Kalimantan. The peak-value areas were located in the Tsushima Strait (above 2.0 cm/a), the waters of the Ryukyu Islands (above 2.0 cm/a), the Beibu Gulf (above 1.5 cm/a) and the Gulf of Thailand (approximately 1.0 cm/a).

In SON, large areas showed a significant increase in SWH. Regions without a significant change were mainly distributed in the southeast of the Indo-China Peninsula and east of the Philippines. The regions with a relatively strong increase were located in the Tsushima Strait (3.0–3.5 cm/a) and around the Dongsha Islands (above 3.5 cm/a).

In DJF, large areas showed a significant increase, and the areas with a relatively strong increase were distributed in the Tsushima Strait (above 4 cm/a) and the northern South China Sea (2.5–4.0 cm/a). The areas without a significant change were mainly located in the small oval-shaped water body to the north of the Philippines.

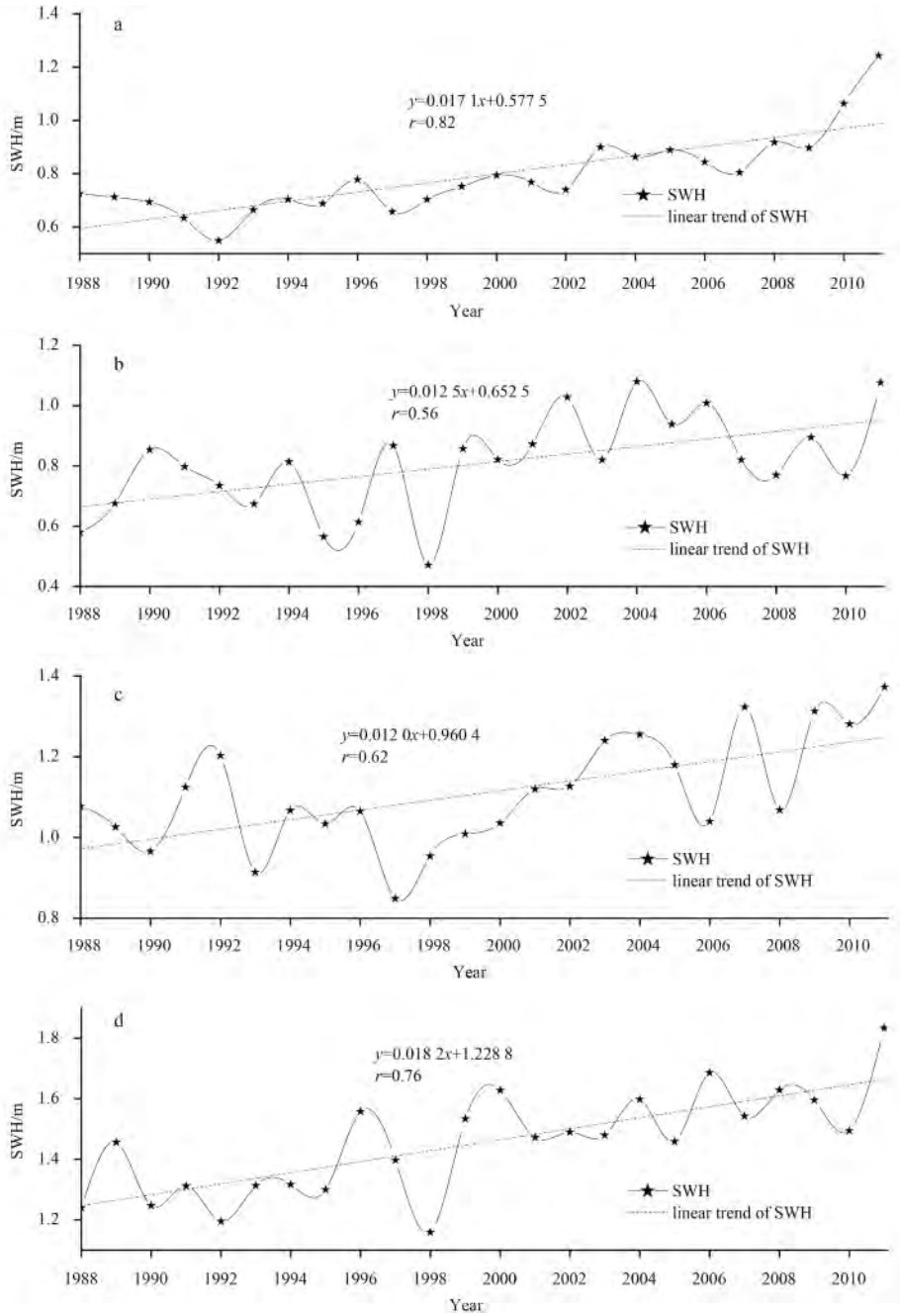

Fig. 4. Long-term trends in the China's seas SWH in MAM (a), JJA (b), SON (c) and DJF (d).

3.4 *Dominant season of the long-term trends in different water bodies*

Comparing the annual variations to the seasonal characteristics of the variations in the WS and the SWH, we found that the variations in the SWH and WS in different water bodies depend on the seasons, as listed in Tables 1 and 2.

From Table 1, the Tsushima Strait and the Taiwan Strait have the strongest increases in WS. The greatest WS increases occur in the Tsushima Strait in DJF and in the Taiwan Strait in MAM and DJF; both regions have winds of 12–18 cm/(s·a). Overall, DJF had the greatest increase in WS, followed by MAM in most China's seas. JJA and SON had the greatest trends in small areas, such as the Bohai Sea and the Gulf of Thailand.

From Table 2, the increases in the SWH in most areas of the China's seas were very similar to the increases in the WS, particularly in DJF. MAM has the second-largest trends, while small areas have strong trends in SON. The China's seas are located along the edge of the Pacific Ocean. This area is significantly influenced by monsoons, and mixed waves are dominated by wind sea (wind-controlled waves); the swell composes only a small portion of the mixed wave. The areas with a strong increase in the SWH were mainly located in the Tsushima Strait and the Taiwan Strait. The trend in the Tsushima Strait is most apparent in DJF, while the trend in the Taiwan Strait significantly increases in DJF, MAM and SON.

Li (1990) and Chen et al. (2000) noted that the interannual variability in the East Asian monsoon is related to the ENSO. The East Asian monsoon is always weak during El Nino and relatively

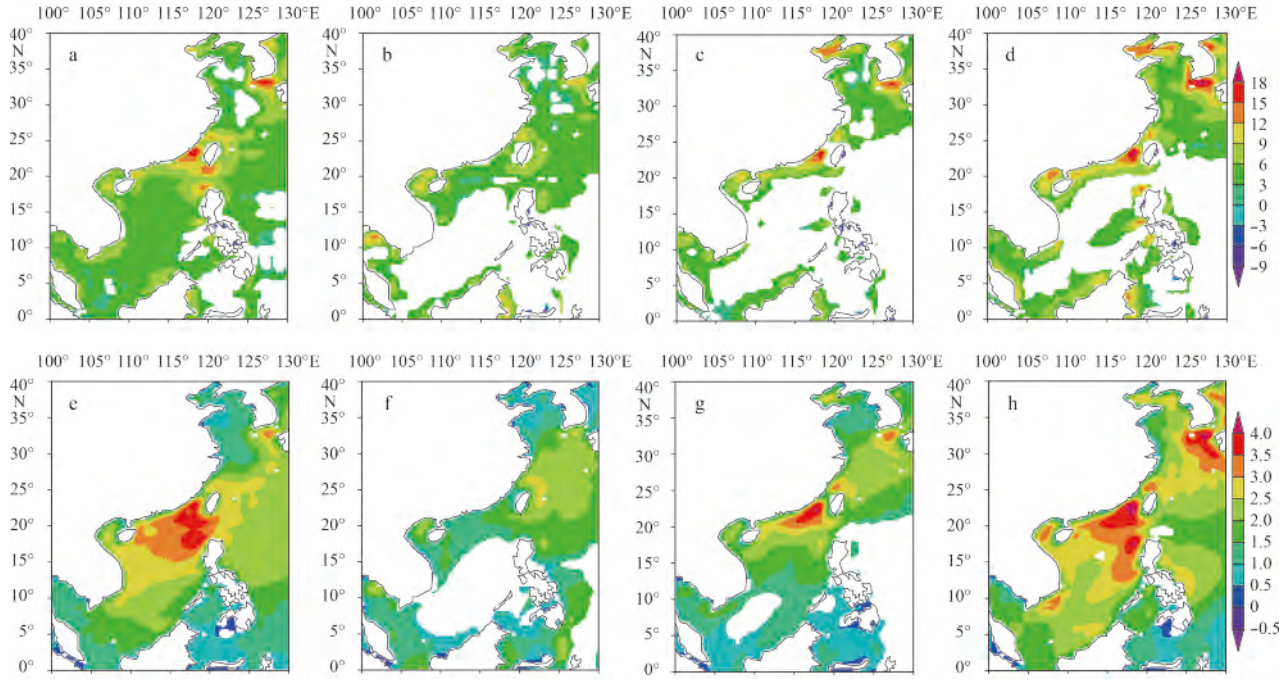

Fig. 5. Long-term trends in the sea surface WS (a–d, cm/(s·a)) and SWH (e–h, cm/a) in MAM, JJA, SON and DJF from 1988 to 2011 in China's seas. Only trends significant at the 95% level are shown.

Table 1. Contrast of the long-term trend in the WS (cm/(s·a)) in various regions

Area	MAM	JJA	SON	DJF	Annual	Dominant season
Bohai Sea	6–9	3–6	9–15	9–15	9–12	SON, DJF
Northern Yellow Sea	3–6	4–6	6–9	9–12	6–9	DJF
Tsushima Strait	12–15	6–9	9–15	12–18	1218	DJF
Ryukyu Islands waters	6–9	3–6	3–6	3–6	3–6	MAM
North area of Taiwan Strait	9–12	6–9	6–9	9–12	9–12	MAM, DJF
South area of Taiwan Strait	12–18	3–6	9–15	12–18	9–15	MAM, DJF
Northern South China Sea	6–9	3–6	6–9	6–12	6–9	DJF
Beibu Gulf	6–9	6–12	6–12	9–15	6–12	DJF
Gulf of Thailand	3–6	9–12	6–9	3–6	3–9	JJA

Table 2. Contrast of the long-term trend in the SWH (cm/a) in various regions

Area	MAM	JJA	SON	DJF	Annual	Dominant season
Bohai Sea	1.0–1.5	0.5–1.0	2.0–2.5	2.0–2.5	1.5–2.0	DJF, SON
Northern Yellow Sea	1.0–1.5	0.5–1.0	1.5–2.0	2.5–3.0	1.5–2.0	DJF
Tsushima Strait	2.5–3.0	2.0–2.5	2.5–3.5	3.0–4.0	3.0–4.0	DJF
Ryukyu Islands waters	2.0–3.0	2.0–2.5	2.0–2.5	2.5–3.0	3.0–3.5	DJF
North area of Taiwan Strait	2.5–3.0	2.0–2.5	2.5–3.5	2.5–3.5	3.0–3.5	SON, DJF
South area of Taiwan Strait	3.0–4.0	1.5–2.0	3.5–4.0	3.5–4.0	3.5–4.0	DJF, MAM, SON
Northern South China Sea	2.5–3.5	1.0–1.5	2.0–3.0	2.5–3.5	3.0–3.5	MAM, DJF
Beibu Gulf	2.0–2.5	1.5–2.5	1.5–2.5	2.5–3.5	2.5–3.0	DJF
Gulf of Thailand	1.0–1.5	1.0–2.0	1.0–1.5	1.5–2.0	1.5–2.0	DJF

strong during La Nina. Mirzaei et al. (2013) found that the SWH in the South China Sea correlates negatively with the Niño3.4 index during winter, spring and autumn and positively during the summer monsoon. The effect of the ENSO should explain the variation in the China's seas WS and SWH. Extremely timely research presented by Zheng and Li (2015) shows that the wave power density and the SWH in the China's seas and adjacent waters have exhibited significant increases over the past two decades. The authors also noted that this phenomenon is likely due to the increasing gale occurrence and ENSO.

4 Conclusions

This study exhibited the seasonal characteristics of the long-term trends in the China's seas WS and SWH based on a 24 a

(1988–2011) CCMP wind data set and a 24 a hindcast wave dataset obtained with the WAVEWATCH-III (WW3) wave model forced by the CCMP wind data. The results indicate the following.

(1) From 1988 to 2011, the China's seas WS and SWH exhibited significant increases overall, i.e., 3.38 cm/(s·a) and 1.3 cm/a, respectively.

(2) During 1988–1996, the WS changed slowly. After 1996, the WS decreased rapidly and dropped to a minimum in 1998. From 1998 to 2003, the WS increased rapidly. For 2004–2011, the variation was relatively stable. The year of 2010 was unusual. The variation in SWH was consistent with that of the WS overall.

(3) The increase in the China's seas WS was strongest in MAM (4.19 cm/(s·a)), followed by DJF (3.82 cm/(s·a)), JJA (3.21 cm/(s·a)), and SON (2.42 cm/(s·a)). The increase in the SWH (1.82 cm/a) was strongest in DJF, followed by MAM (1.71 cm/a), JJA (1.25 cm/a), and SON (1.20 cm/a).

(4) The areal extent of the significant increase in the WS was largest in MAM; the area decreased in JJA and DJF until reaching the smallest extent in SON. In contrast to the WS, almost all of the China's seas areas exhibited significant increases in SWH in MAM and DJF, and the area was slightly smaller in JJA and SON. The WS and the SWH in the Bohai Sea, the Yellow Sea, the East China Sea, the Tsushima Strait, the Taiwan Strait, the northern South China Sea, the Beibu Gulf, and the Gulf of Thailand exhibited a significant increase in all seasons, while only a few sporadic water bodies show a significant decrease.

(5) The variations in the SWH and the WS in different water bodies depended on the season. The areas with a strong increase usually appeared in DJF.

References

Atlas R, Hoffman R N, Ardizzone J, et al. 2011. A cross-calibrated, multiplatform ocean surface wind velocity product for meteorological and oceanographic applications. American Meteorological Society, 92: 157–174, doi: 10.1175/2010BAMS2946.1

Chen W, Hans F G, Huang R H. 2000. The interannual variability of East Asian winter monsoon and its relation to the summer monsoon. Advances in Atmospheric Sciences, 17: 46–60

Chu P C, Qi Y Q, Chen Y C, et al. 2004. South China Sea wind-wave characteristics: Part I. Validation of WAVEWATCH-III using TOPEX/Poseidon data. Journal of Atmospheric and Oceanic Technology, 21: 1718–1733

Earl N, Dorling S, Hewston R, et al. 2013. 1980–2010 variability in U.K. surface wind climate. Journal of Climate, 26: 1172–1191

Gower J F R. 2002. Temperature, wind and wave climatologies, and trends from marine meteorological buoys in the northeast Pacific. Journal of Climate, 15: 3709–3718

Guillaume D, Bertin X, Taborda R. 2010. Wave climate variability in the North-East Atlantic Ocean over the last six decades. Ocean Modelling, 31(3–4): 120–131

Gulev S K, Grigotieva V. 2006. Variability of the winter wind waves and swell in the North Atlantic and North Pacific as revealed by the voluntary observing ship data. Journal of Climate, 19: 5667–5685

Han S Z, Zhang H R, Zhang Y X. 2014. A global study of temporal and spatial variation of SWH and wind speed and their correlation. Acta Oceanologica Sinica, 33(11): 48–54

Huang G, Qu X, Hu K M. 2011. The impact of the tropical Indian Ocean on South Asian High in boreal summer. Advances in Atmospheric Sciences, 28(2): 421–432

Li C Y. 1990. Interaction between anomalous winter monsoon in East Asia and El Nino events. Advances in Atmospheric Sciences, 7(1): 36–46

Mirzaei A, Tangang F, Juneng L, et al. 2013. Wave climate simulation for southern region of the South China Sea. Ocean Dynamics, 63(8): 961–977

Ren L, Yang J S, Zheng G, et al. 2015. Wave effects on the retrieved wind field from the advanced scatterometer (ASCAT). Acta Oceanologica Sinica, 34(1): 79–84

Soomere T, Raamet A. 2011. Long-term spatial variations in the Baltic Sea wave fields. Ocean Science, 7: 141–150

Suarez J M, Cicin-Sain B, Wowk K, et al. 2013. Ensuring survival: oceans, climate and security. Ocean and Coastal Management, 90: 27–37

Young I R, Zieger S, Babanin A V. 2011. Global trends in wind speed and wave height. Science, 332 (6028): 451–455

Zheng Y, Jiang X W, Song Q T, et al. 2014. Coastal wind field retrieval from polarimetric synthetic aperture radar. Acta Oceanologica Sinica, 33(5): 54–61

Zheng C W, Li C Y. 2015. Variation of the wave energy and significant wave height in the China Sea and adjacent waters. Renewable and Sustainable Energy Reviews, 43: 381–387

Zheng C W, Pan J. 2014. Assessment of the global ocean wind energy resource. Renewable and Sustainable Energy Reviews, 33: 382–391

Zheng C W, Pan J, Huang G. 2014. Forecasting of the China Sea ditching probability using WW3 wave model. Journal of Beijing University of Aeronautics and Astronautics, 40(3): 341–320

Zheng C W, Pan J, Li J X. 2013. Assessing the China Sea wind energy and wave energy resources from 1988 to 2009. Ocean Engineering, 65: 39–48

Zheng C W, Shao L T, Shi W L, et al. 2014. An assessment of global ocean wave energy resources over the last 45 a. Acta Oceanologica Sinica, 33(1): 92–101

Zheng C W, Zhou L, Huang C F. 2013. The long-term trend of a sea surface wind speed and a (wind wave, swell, mixed wave) wave height in global ocean during the last 44 a. Acta Oceanologica Sinica, 32(10): 1–4